Article

Not peer-reviewed version

Optimization of In-Situ Formation of a TiC Nanohybrid by Mechanical Alloying Using Stearic Acid and CNTs as Carbon Sources

María Luisa Camacho-Ríos *, Guillermo Herrera-Pérez, Marco Antonio Ruiz Esparza-Rodríguez, Raúl Pérez-Bustamante, John Edison García-Herrera, Daniel Lardizabal-Gutiérrez, José Antonio Betancourt-Cantera

Posted Date: 31 October 2023

doi: 10.20944/preprints202310.2025.v1

Keywords: Nanocomposites; mechanical alloying; process control agent; carbon nanotubes; titanium

Article

Optimization of In-Situ Formation of a TiC Nanohybrid by Mechanical Alloying Using Stearic Acid and CNTs as Carbon Sources

María Luisa Camacho-Ríos [1,2,*], Guillermo Herrera-Pérez [3], Marco Antonio RuizEsparza-Rodriguez [2], Raúl Pérez-Bustamante [1], John Edison García-Herrera [4], Jose Antonio Betancourt-Cantera [1] and Daniel Lardizabal-Gutierrez [2]

[1] Corporación Mexicana de Investigación en Materiales S.A. de C.V. (COMIMSA), Ciencia y Tecnología 790, Saltillo 400, 25290 Saltillo, Coahuila, México; jbetancourt@comimsa.com; raul.perez@comimsa.com.
[2] Centro de Investigación en Materiales Avanzados (CIMAV), Miguel de Cervantes 120, 31109, Chihuahua, Chih., México; marco.ruiz@cimav.edu.mx; daniel.lardizabal@cimav.edu.mx.
[3] CONAHCYT-Centro de Investigación en Materiales Avanzados (CIMAV), Miguel de Cervantes 120, 31109, Chihuahua, Chih., México; guillermo.herrera@cimav.edu.mx.
[4] CONAHCYT-CIATEQ A.C. Centro de Tecnología Avanzada, Eje 126 No.225, Industrial San Luis, San Luis Potosí, 78395, México; john.garcia@ciateq.mx.
* Correspondence: luisa.camacho@cimav.edu.mx

Abstract: The current work shows the optimization in the preparation of nanosized titanium carbide (TiC) in-situ through mechanical alloying (MA). Metallic titanium (Ti) powders, along with two carbon sources, carbon nanotubes (CNTs), and stearic acid (SA), were used to reduce the particle size using a high-energy Spex800 mill. The combined use of 2 wt % of these carbon sources and n-heptane as a liquid process control agent (PCA) proved crucial in generating nanoscale powder composites through a simple and scalable synthesis process within a 4-hour timeframe. The use of 20 wt % of both carbon sources was compared to determine the ability of CNTs to form carbides and the decomposition of PCAs during mechanical milling. The structure and morphology of the composites and starting materials were evaluated through x-ray diffraction (XRD), Raman spectroscopy, scanning electron microscopy (SEM), and transmission electron microscopy (TEM).

Keywords: Nanocomposites; mechanical alloying; process control agent; carbon nanotubes; titanium

1. Introduction

Titanium Carbide (TiC) is characterized as one of the metal carbides with high hardness (28-35 GPa), a high melting point (3067-3340ºC), great resistance to abrasion, high chemical stability, thermal conductivity, and electrical conductivity [1]. TiC is commonly used as a reinforcement in other materials such as aluminum, titanium, and their alloys [2, 3]. In recent years, various synthesis methods have been studied, including carbo-thermal reduction, electrospinning, high-temperature self-propagation (SHS), and chemical vapor deposition [4, 5]. This is because its production requires high temperatures, incurring high costs, prompting the industry to explore different alternatives.

Mechanical alloying is a method that allows the synthesis of materials with different properties, resulting in alloys that are stronger and lighter, making them attractive for the aerospace and automotive industries that demand such materials [6]. The steps in this method are optimized, eliminating the need for subsequent washes or heat treatments. TiC synthesis begins with elemental materials, Ti powders, and different carbon sources such as graphite, CNTs, activated carbon, etc [7, 8]. The goal is to control the microstructure, design the composites, distribute the carbon source in the metal matrix, and achieve chemical interaction, allowing the metal to wet the graphite and form carbides.

 doi:10.20944/preprints202310.2025.v1

The formation of TiC is an exothermic process, and the phase is synthesized layer by layer through combustion or thermal explosion [9]. In the synthesis process through MA, organic surfactants or process control agents (PCAs) are used as lubricants to achieve a balance between material fracture and cold welding, improving process efficiency and preventing powder agglomeration resulting from milling. Nouri et al. in 2013 [10] conducted a study on the effect of PCAs in the mechanical milling process. They describe that there are solid and liquid PCAs, with the most commonly used being stearic acid (SA), ethylene bis stearamide (BIS), ethanol, methanol, hexane, oleic acid, etc. PCAs are absorbed onto the surface of particles, and during MA, they decompose into carbon, hydrogen, oxygen, and nitrogen. The combination of these elements with milling materials can lead to the formation of carbides, hydrides, oxides, and nitrides.

The decomposition of the PCA can be considered beneficial in various studies when the intention is to reduce metallic oxides [11, 12]. Another commonly reported decomposition of the PCA is that of carbon [13, 14]. The reaction of metals with liquid PCAs derived from hydrocarbons such as hexane and n-heptane has been studied to evaluate their effect on particle size reduction. In both studies, XRD results revealed the appearance of peaks corresponding to the formation of a new phase, suggesting that chemical reactivity increases during milling, favoring the transition of metals with carbon in carbide formation [15, 16]. The decomposition of PCA by milling offers the dual advantage of being a tool that allows in-situ carbide formation and a reduction in particle size in the nanometric range.

The motivation for this work is to synthesize in-situ TiC composites using the mechanical alloying technique. In the preparation, Ti powders with a hexagonal crystalline structure are considered, along with two carbon sources. The first is stearic acid, with the dual purpose of analyzing its effect as a PCA and simultaneously as a carbon source in TiC formation. The second source is CNTs. The TiC composites were structurally characterized by x-ray diffraction (XRD) and high-resolution transmission electron microscopy (HR-TEM). The microstructure was analyzed by scanning electron microscopy (SEM) and transmission electron microscopy (TEM). Chemical analysis was monitored through energy dispersive x-ray (EDX) mappings, while Raman band analysis complemented the characterization of this material.

2. Materials and Methods

Combinations of Alpha Aesar titanium powders (Ti, 99.5%) and two different carbon sources (CS) were prepared. Stearic acid (SA) from Sigma-Aldrich ($C_{18}H_{36}O_2$, 95%) and carbon nanotubes (CNTs) synthesized according to the literature [17-19] were utilized as carbon sources. N-heptane (FC) from Jalmek (C7H16, 98.5%) was employed as a process control agent. Table 1 presents the nomenclature of the titanium and carbon source combinations used at different percentages, 2 and 20 wt % in weight of the elements that compose them [7, 20]. The milling process was carried out in a high-energy Spex8000 mill, with a ball-to-powder ratio of 5:1, and a milling time of 4 hours in an argon atmosphere. 1.0 ml of process control agent was used.

Table 1. The notation used to distinguish the samples with titanium and the different carbon sources employed in the mechanical alloying technique to obtain in-situ TiC.

Carbon Sources	Name	Ti (wt %)	CS (wt%)	Ti (g)	FC (g)
SA	A1	98	2	7.84	0.16
	A2	80	20	6.4	1.6
CNTs	B1	98	2	7.84	0.16
	B2	70	30	6.4	1.6

The x-ray

The x-ray diffraction (XRD) technique was employed to determine the structure of all synthesized materials and to ascertain the average crystallite size of the compound. The x-ray diffractometer used was the Panalytical model XPert PRO. The conditions for obtaining the diffraction patterns were as follows: 2θ (°) in a range of 5 - 90; step size (◦): 0.0131; step time (min): 18. The x-ray diffraction patterns were refined using the Fullprof program.

Raman spectroscopy was utilized to identify the type of carbon allotrope and determine its structural characteristics in the graphitic network. Additionally, it was employed to identify the

 doi:10.20944/preprints202310.2025.v1

characteristic bands of TiC. The spectroscope used was from Horiba, model LabRam HR Vis-633, with a He-Ne laser source at 632.58 nm. The conditions for obtaining Raman spectra of the samples were as follows: scanning range (cm^{-1}): 200 to 1000 cm^{-1}.

The scanning electron microscopy (SEM) technique was employed to evaluate the morphology, while the chemical composition was monitored using energy dispersive x-ray (EDX) of the samples. The SEM used was the Hitachi model JEOL JSM-7401F. A voltage of 10 kV was utilized during image collection. The average particle size of the synthesized materials and their morphology were determined using a transmission electron microscope (TEM), model JEOL JEM2200FS. Sample preparation for TEM involved dispersing nanoparticles in isopropanol through a sonication process for 1 hour. A drop was then deposited onto a Lacey carbon film on a 300 Cu mesh grid.

3. Results and Discussion

3.1. X-ray Diffraction (XRD) Analysis

In Figure 1, the x-ray diffraction patterns for powders obtained from mechanical milling for a duration of 4 hours are observed. Samples A1 and B1 retain the crystalline structure of the initial titanium phase identified with the crystallographic chart (ICSD 00-044-1294). This chart is associated with a hexagonal crystalline structure with the Fm-3m (225) space group. The x-ray diffraction pattern of Ti is also included in this figure for comparison between the diffraction peaks of samples A1 and B2. For sample A2, broadened signals are observed, indicating that the material is not crystallized. Meanwhile, the x-ray diffraction pattern for sample B2 suggests a majority phase of TiC with the presence of a secondary phase associated with Ti. Suzuki et al; 1995 [16] investigated the formation of metastable intermediate phases that occur after milling Ti hcp and n-heptane in a planetary mill. The authors conducted a dry pre-milling for 12 hours and a wet milling for 20 hours (n-heptane), followed by heat treatment at different temperatures (from 693 K to 1073 K). Their results show the formation of TiC accompanied by a second phase associated with Ti fcc. The authors argue that as the annealing temperature increases, Ti hcp re-emerges. In their interpretation, they suggest that this behavior is reversible. During mechanical milling, the dissolution of C and H occurs. They describe the intermediate phase as a supersaturated solution of C and H. With the increase in temperature, H dissolves, allowing the formation of TiC.

The x-ray diffraction patterns of samples A1, B1, and A2 exhibit significantly broadened reflections, which can be attributed to the powders being in the nanoscale range. Subsequently, the average crystallite size was determined using the Scherrer equation with the assistance of the High Score X pert program [21].

The results suggest an average crystallite size of 98.4 nm for titanium as powders in the initial stage. After milling, there was an achieved reduction in the average crystallite size in samples A1 and B1 of 24.2 nm and 18.7 nm, respectively. For sample B2, an average crystallite size of 34.3 nm was determined. Key conclusions derived from this analysis include the possibility of a phase transformation from hcp to fcc using the mechanical milling technique, followed by heat treatment. Additionally, a reduction in the crystallite size is observed.

Bolokang et al; in 2015 [22] mixed Ti hcp with stearic acid at a ratio of 5 wt % for a duration of 15 hours, followed by sintering and quenching at 1200 ºC. In their results, the authors reported a size of 73 nm for unmilled titanium and 47 nm after 15 hours [23, 24]. These results suggest that the combination of liquid and solid process control agents allows for a reduction in the material's surface tension, favoring a decrease in its size in relatively short milling times.

Preprints (www.preprints.org) | NOT PEER-REVIEWED | Posted: 31 October 2023 doi:10.20944/preprints202310.2025.v1

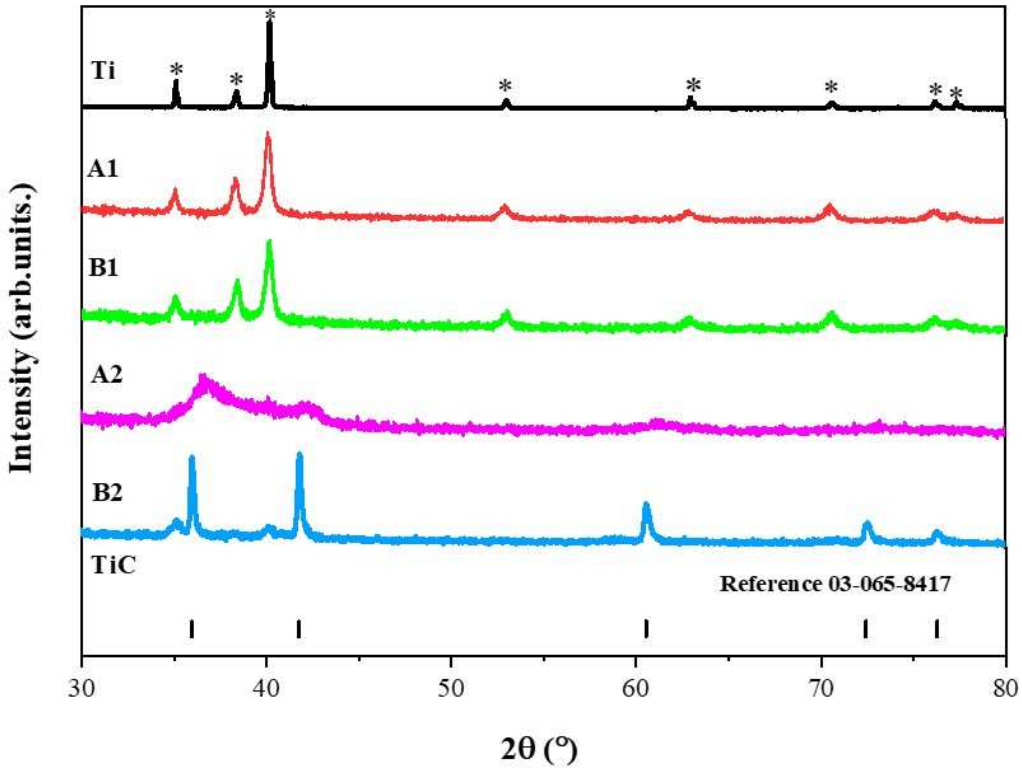

Figure 1. Indexing of x-ray diffraction patterns for samples obtained from milling for a duration of 4 hours. Samples A1 and B1 demonstrate the formation of Ti, whereas sample B2 is predominantly TiC with the presence of Ti. Sample A2 exhibits signals indicating powders with an amorphous character.

3.1.1. Rietveld Method Refinement

To determine the parameters of the unit cell in the sample where TiC was predominantly obtained, refinement of the diffraction patterns was carried out using the Rietveld method implemented in the Fullprof program. Panel a of Figure 2 presents a comparison between the experimental diffraction pattern (black line with symbols, Y_{obs}) and the calculated diffraction pattern (continuous red line, Y_{calc}). In this figure, the residual line (continuous black line, Y_{obs}-Y_{calc}) and Bragg positions are also depicted. The diffraction pattern for sample B2 reveals the presence of two phases, predominantly TiC and Ti, which were considered in the refinement. The presence of the second phase associated with Ti is a remnant that we consider did not fully react [7, 8, 25]. Panel b shows the titanium carbide phase identified with the crystallographic chart (ICSD 03-065-8417) which is associated with the cubic-type structure.

Preprints (www.preprints.org) | NOT PEER-REVIEWED | Posted: 31 October 2023 doi:10.20944/preprints202310.2025.v1

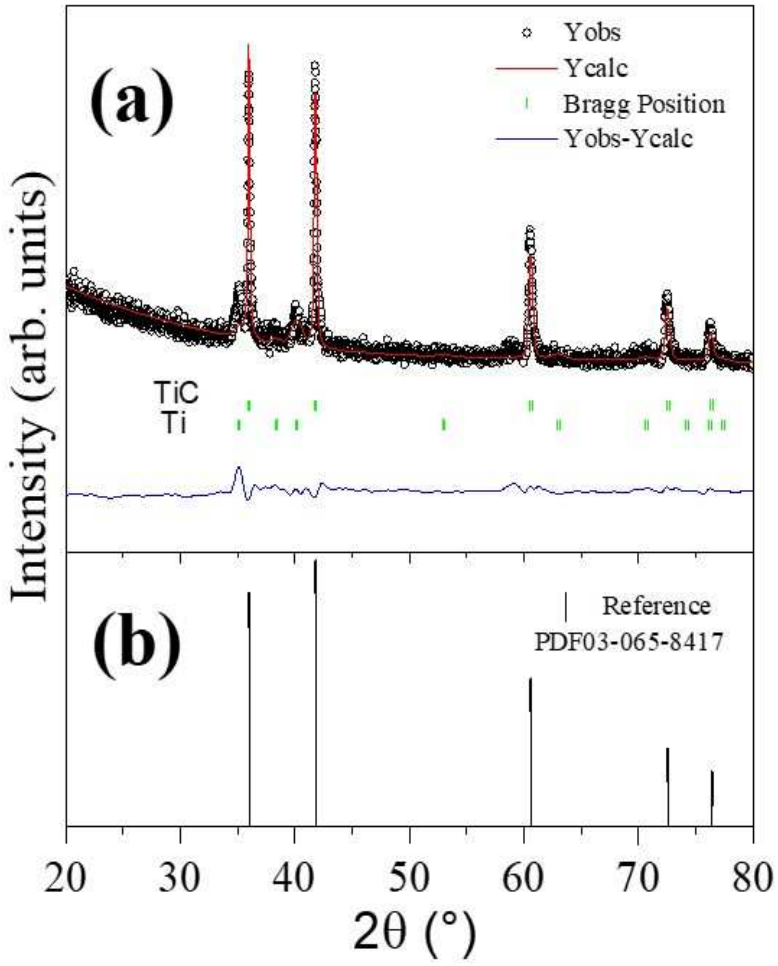

Figure 2. (a) Comparison between the experimental diffraction pattern (Yobs) and the refined pattern (Ycal) using the Rietveld method for sample B2. (b) Reference pattern for the cubic-type structure similar to NaCl (03-065-8417 pdf).

Table 2. summarizes the refined parameters obtained by considering the space groups for TiC and Ti.

Samples	Lattice parameters (Å)	Phase	Phase (%)	Rp (%)	Rwp (%)	Rexp (%)	Vol (Å)³	χ^2
TiC	a=b=c=4.320(9)	bcc	84.73	17.0	24.1	11.29	80.676	4.54
Ti^{2+}	a=b=2.951(4) c=4.688(5)	hcp	15.27				35.371	4.54
Reference PDF03-065-8417	a=b=c=4.320(9)	bcc	100				80.543	NA

3.2. Scanning ElecScanning electron microscopy (SEM)

In Figure 3, the morphology of the initial materials is depicted, corresponding to Ti and CNT particles. Additionally, an inset shows a count of 200 particles to determine the average particle size. The counting was conducted using the Image J program. The histogram, along with its analysis employing a log-normal fit using the iterative Levenberg-Marquardt method, was performed with the Origin program.

Morphological features observed in Figure 3a reveal that Ti powders exhibit a non-uniform polygonal shape resembling flakes, with an average particle size of 10.98 ± 0.27 μm. In panel b, a micrograph of CNTs is presented, showcasing their typical long and slender spaghetti-like form, which is prone to clustering.

Preprints (www.preprints.org) | NOT PEER-REVIEWED | Posted: 31 October 2023 doi:10.20944/preprints202310.2025.v1

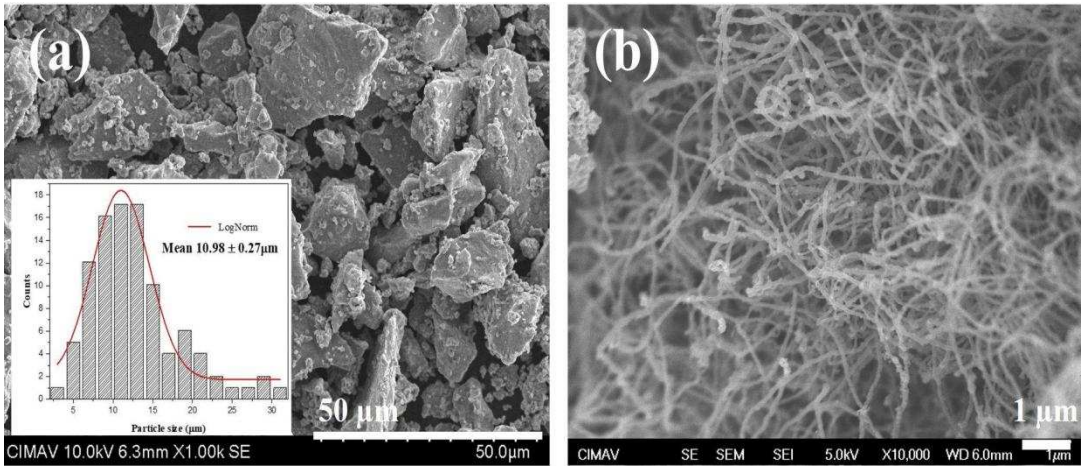

Figure 3. SEM micrographs of starting materials for: (a) Titanium particle morphology. The inset shows the average particle size obtained by the analysis of histogram using log-normal fitting; (b) Carbon nanotubes morphology and distribution.

At the bottom of the panel are samples A2 and B2 with a carbon content of 20 wt %. In sample A2, irregularly shaped particles smaller than 10 µm are observed, while in sample B2, finer flake-like shapes predominate. Both samples show the presence of the TiC phase (Figure 1). In literature [27, 28], it is reported that during MA, ductile Ti particles envelop brittle particles, in this case, C. When the balance between fracture and cold welding is lost, agglomerate size grows due to the high surface energy produced on the new surface. This new surface results from particle fracture, compressing and increasing intimate contact between atoms, accelerating C diffusion into titanium, inducing forging work [27, 28].

In Figure 4, the sample A2, the combination of 20 wt % stearic acid and n-heptane has a dual effect: i) acting as a lubricant and ii) when welding dominates over fracture. This phenomenon is attributed to the decomposition of stearic acid, and n-heptane during this stage acts as a carbon source, leading to a TiC-deficient phase, as observed in Figure 1. Conversely, for sample B2 with 20 wt % CNTs, in the first stage, CNTs and n-heptane act as lubricants, reducing particle size. Milling generates interstitial defects and dislocations in both materials, increasing their chemical reactivity. In this stage, CNTs are introduced into Ti layers, and as temperature rises during milling, TiC formation occurs. If the temperature decreases, it can be attributed to the partial transformation of reactants, developing intimate contact between CNTs and Ti [29, 30].

Preprints (www.preprints.org) | NOT PEER-REVIEWED | Posted: 31 October 2023 doi:10.20944/preprints202310.2025.v1

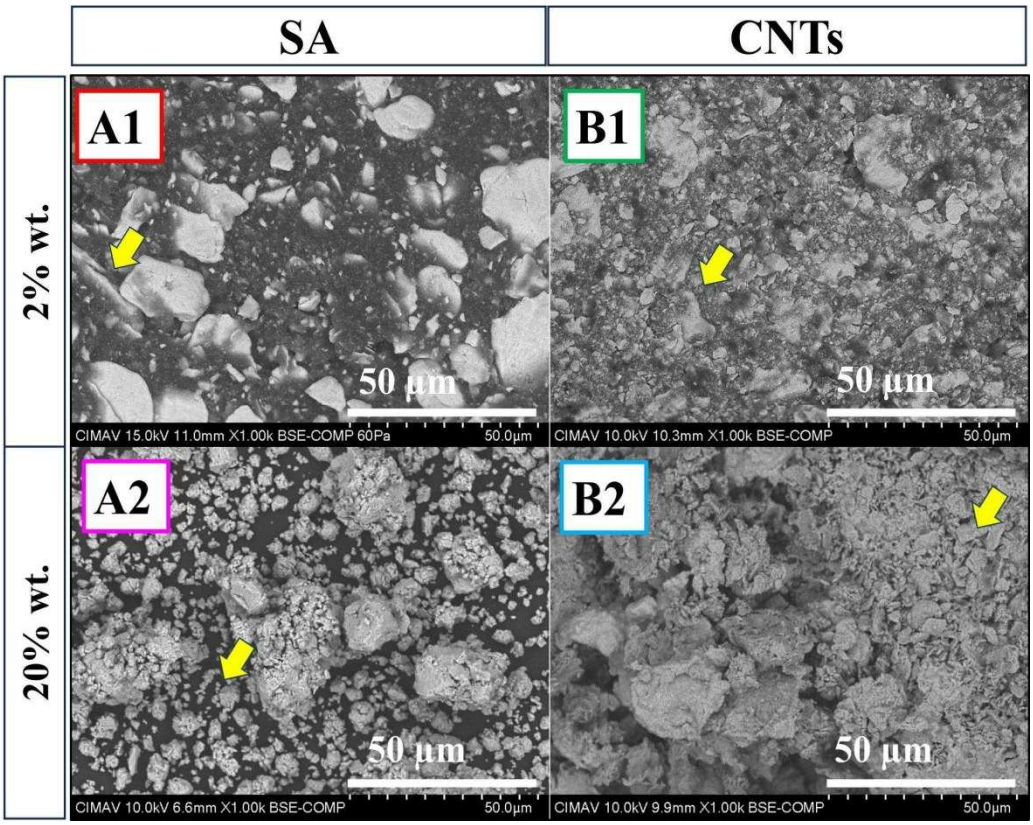

Figure 4. SEM micrographs of morphological behavior of powders prepared by mechanical alloying TiC.

3.2.1. Elemental Analysis- EDS Elemental Mapping

During mechanical alloying, there is a possibility of powder contamination due to milling conditions or interstitial impurities present in the air within the vial (nitrogen, oxygen). The estimation of atomic percentages of Ti, C, and the presence of O may be due to exposure to the environment, leading to the absorption of oxygen species like hydrated oxides (OH, O^-). Another potential cause is the components of the PCA when used in high quantities during milling [13, 31]. All metals are inherently reactive and can easily combine with elements such as hydrogen, oxygen, carbon, and nitrogen to form hydrides, oxides, carbides, and nitrides [32].

In Figure 5, SEM-EDS elemental maps of samples A1 and B1 are shown, revealing a uniform chemical distribution. The results suggest that these elements are not present in interstitial sites or in the form of oxides or carbides. In sample A2, the absence of C is observed, possibly because it was embedded within the Ti layers. Conversely, in sample B2, the distribution of elements indicates the formation of the TiC phase, as evidenced by XRD analysis (Fig. 1).

Preprints (www.preprints.org) | NOT PEER-REVIEWED | Posted: 31 October 2023 doi:10.20944/preprints202310.2025.v1

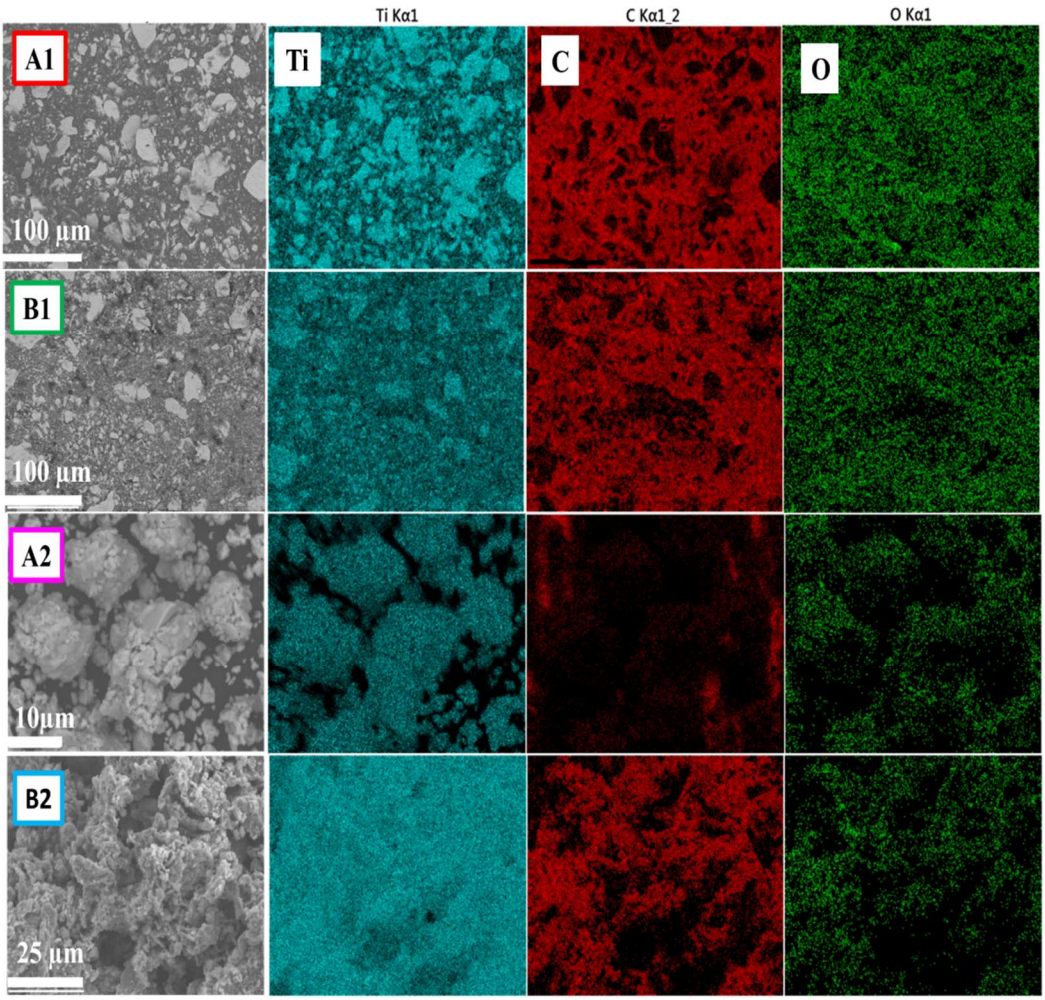

Figure 5. SEM-EDS map of element distribution (titanium, oxygen and carbon) in the alloy powders TiC.

3.3. High-Resolution Transmission Electron Microscopy (HR-TEM)

Figure 6 presents HR-TEM micrographs for sample B2, which predominantly exhibits the TiC phase. HR-TEM analysis provides information on the morphology, structure, and size of particles. In Figure 6a, a CNT with a section showing defects (yellow square), possibly due to the milling process, is observed. Additionally, a framework structure composed of TiC particles can be seen. This type of formation is similar to that described by Saba et al; in 2017 [23]. In their study, they explain two possible sources of carbon when using CNTs for TiC synthesis: i) defects in the CNT walls and ii) deformed parts detached from the CNT walls. Figure 6b is a schematic visualization containing both mechanisms for the formation of TiC nanocrystals. This visualization was created using VESTA software [33]. The arrows indicate the direction of Ti particles reacting on the CNT walls, forming nanoblocks around it. During milling, Ti particles are introduced into the CNTs, mainly at their ends containing defects [9, 26].

 doi:10.20944/preprints202310.2025.v1

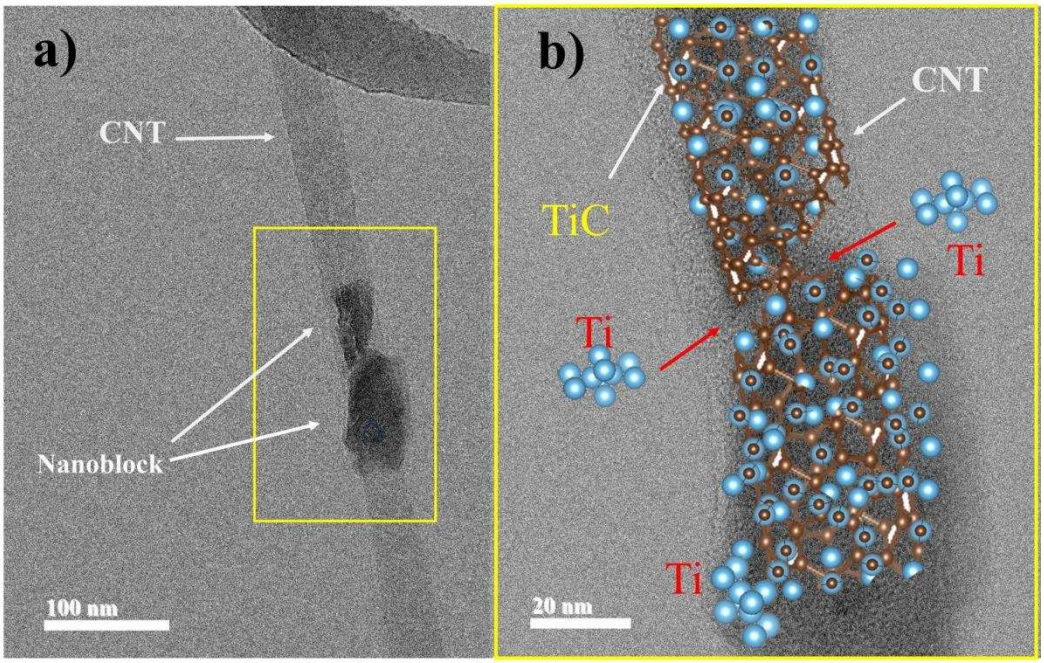

Figure 6. HR-TEM micrographs of CNT with TiC. a) Nanoblock of TiC developed in a CNT, b) schematic visualization of the formation mechanism of in-situ TiC around a CNT using VESTA software.

Continuing with the microstructural analysis of TiC nanoparticles, panel a of Figure 7 presents a representative HR-TEM micrograph. In this micrograph, two highlighted regions can be observed. The first region, marked in blue, shows two polygonal-shaped particles merging to form a lump-like structure [23], corresponding to TiC. In the second region, marked in yellow, an elongated microstructure corresponding to CNTs can be observed. Figure 7b provides a magnification of a CNT section, indexed using Digital Micrograph software [34] and identification card No. 00-041-1487. The indexing associates an interplanar distance of 0.34 nm with the (0 0 2) plane. Figure 7c is a section within the polygonal particle, where a distance of 0.245 nm corresponding to the (111) plane of TiC was obtained, with identification card No. 03-065-8417. Dislocations and folded zones resulting from milling, indicating a plastically deformed structure, can also be observed within the image. It's worth noting the indexed regions exhibiting high crystallinity that persists during the 4-hour milling process.

Preprints (www.preprints.org) | NOT PEER-REVIEWED | Posted: 31 October 2023 doi:10.20944/preprints202310.2025.v1

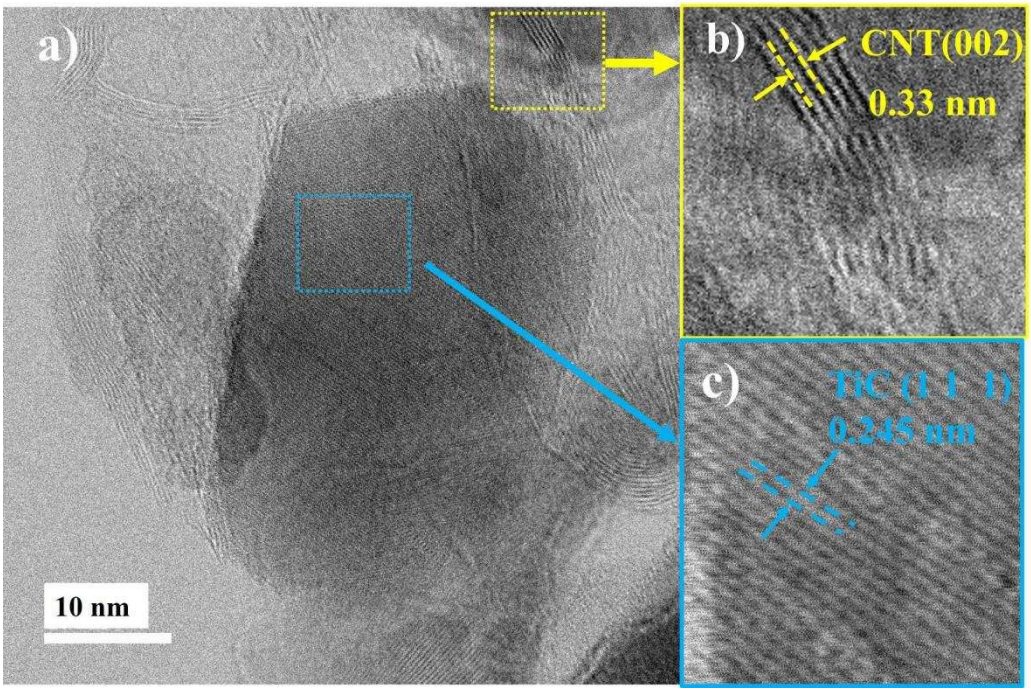

Figure 7. (a) HR-TEM image of TiC (sample B2), Indexing of interplanar distances (b) FFT image corresponding to CNT (yellow box), and (c) FFT image corresponding to TiC (blue box).

3.4. Raman

Raman Spectroscopy was employed to assess the effect of milling on the structure of CNTs and evaluate the influence of carbon sources on TiC formation. Titanium, like most metals, does not exhibit active vibration modes. On the other hand, CNTs, like all carbon allotropes, show two main bands named D and G. The D-band is associated with the concentration of defects or a measure of disorder in C-C bonds within the graphitic network, while the G-band is associated with in-plane vibrations of C-C bonds and the degree of graphitization or metallicity of graphitic materials [35, 36]. Figure 8 contains the Raman spectra of the samples. The Raman spectra can be divided into two regions for description. In the first region (from 200 to 1000 cm^{-1}), three Raman bands associated with the Ti-C bond are observed, centered at 220, 420, and 605 cm^{-1}. These peaks are comparable to those reported in the literature [37, 38].

In the second region (from 1000 to 2000 cm^{-1}), the sample B2 with 20 wt % CNTs exhibits the most intense signals. Regarding the signals from non-reacted carbon, both the D and G signals are detected at 1320 and 1590 cm^{-1}, respectively. These signals are associated with the A_{1g} and E_{2g} vibrational modes of graphitic structures. They are present with low intensity. It is characteristic of high-energy milling that, when milling graphitic compounds like CNTs, the milling process destroys the ordered structure present. This leads to an increase in the intensity of the D band [39].

Sample A1, which contains 2 wt %. SA, reveals broad and low-intensity peaks, contrary to sample B1 with 2 wt%. CNTs, which shows high-intensity peaks for both bands. These results align with the XRD analysis where only Ti was identified. Sample A2 with a 20 wt % SA content contains broad and poorly defined peaks, indicating deficient crystalline synthesis.

Samples synthesized with stearic acid show less definition in the signals, both for TiC and the remaining carbon. The sample with 20 wt %. CNTs is the one where TiC signals are observed with greater definition, consequently indicating a higher synthesis yield.

Preprints (www.preprints.org) | NOT PEER-REVIEWED | Posted: 31 October 2023 doi:10.20944/preprints202310.2025.v1

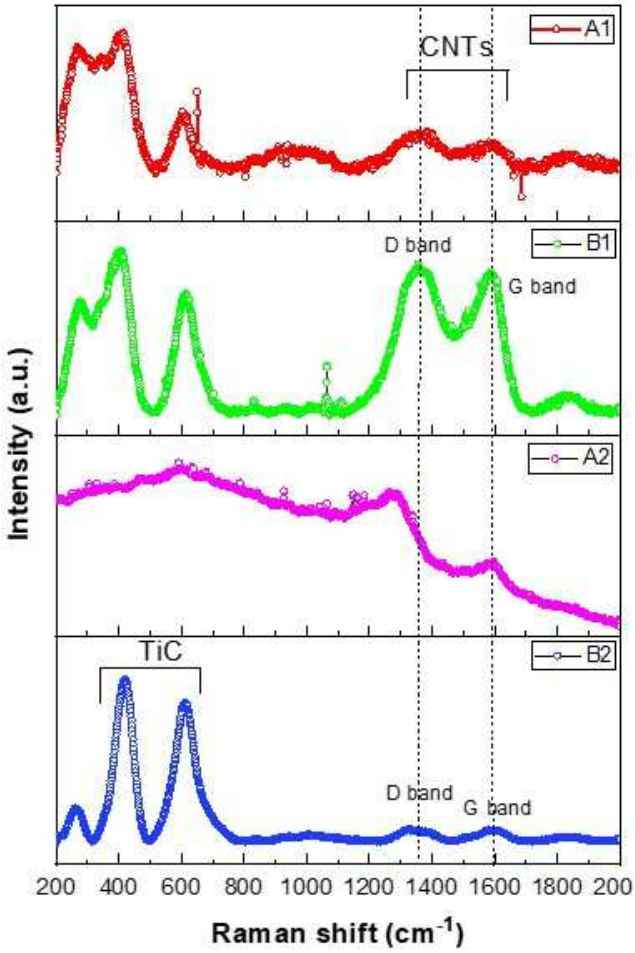

Figure 8. Raman spectra of Ti and C powders milled, samples A1 and A2 (carbon source SA), samples B1 y B2 (carbon source CNTs).

4. Conclusions

We achieved the in-situ formation of TiC nanoparticles through a simple and scalable synthesis using mechanical alloying. The synthesis occurs through the exothermic reaction between Ti and two different carbon sources (stearic acid and carbon nanotubes). The self-propagation reaction between Ti and C developed in a short time of 4 hours. Mechanical milling gradually reduced the particle size of TiC to the nanoscale.

Analysis of XRD patterns using the Rietveld method confirmed the formation of TiC with an fcc structure. Analysis of peak broadening in the XRD patterns through the Scherrer equation suggests an average crystallite size of 15.15 nm and 9.45 nm, respectively.

The morphology observed by SEM suggests that a 2 wt % of stearic acid or carbon nanotubes produces particles in the form of thin and long flakes. In the case of composites with 20 wt % of stearic acid or carbon nanotubes, the particles exhibit a quasi-round shape. These quasi-rounded nanoparticles tend to aggregate to form clusters. In samples A1 and B1, the effect of solid and liquid PCA, which has the ability to reduce particle size, can be observed. However, a 20 wt % of stearic acid or carbon nanotubes, as in samples A2 and B2, is required to consolidate the TiC phase.

TEM micrographs of sample B2 suggest a tendency for TiC nanoparticles to develop in the form of blocks and lumps on the surface and fragmented parts of the nanotubes. Raman spectroscopy analyses indicate a higher synthesis yield of TiC in sample B2. The analysis reveals that the carbon source reacts almost entirely, a finding consistent with the XRD results, quantifying 84.57% of the TiC phase by the Rietveld method. This could be attributed to the fact that carbon nanotubes, with smaller crystal sizes, favor carbide synthesis.

Author Contributions: For research articles with several authors, a short paragraph specifying their individual contributions must be provided. The following statements should be used "Conceptualization, M.L.C.R. and G.H.P.; methodology, D.L.G; software, J.E.G.H. and J.A.B.C; validation, G.H.P., D.L.G. and R.P.B.; formal analysis, .X.; investigation, X.X.; resources, X.X.; data curation, M.A.R.R.; writing—original draft preparation, M.L.C.R.; writing—review and editing, G.H.P and M.L.C.R.; visualization, D.L.G.; supervision. All authors have read and agreed to the published version of the manuscript.

Data Availability Statement: Data are available upon reasonable request.

Acknowledgments: M. L. Camacho-Rios thanks the National Council of Science and Technology for the opportunity to participate in the postdoctoral scholarship project No. 2866844. The authors express gratitude to COMIMSA, CIATEQ, CIMAV, and Nanotech for the infrastructure. Special thanks for data acquisition support to Andrés González (XRD), Karla Campos (SEM), Pedro Pizá (Raman) and L. M. Valdez-Morales (UTCH) for the technical english assistance.

Conflicts of Interest: The authors declare no conflict of interest.

References

1. Dong, B.X.; Qiu, F.; Li, Q.; Shu, S.L.; Yang, H.Y.; Jiang, Q.C. The Synthesis, Structure, Morphology Characterizations and Evolution Mechanisms of Nanosized Titanium Carbides and Their Further Applications. *Nanomaterials* **2019**, 9, 1152.
2. Rao, V.R.; Ramanaiah, N.; Sarcar, M.M.M. Tribological properties of Aluminium Metal Matrix Composites (AA7075 Reinforced with Titanium Carbide (TiC) Particles). *Int. J. Adv. Sci. Technol.* **2016**, 88, 13-26.
3. He, B.; Ma, D.; Ma, F.; Xu, K. Microstructures and wear properties of TiC coating produced by laser cladding on Ti-6Al-4V with TiC and carbon nanotube mixed powders. Ferroelectrics **2019**, 547 217-225.
4. Cochepin, B.; Gauthier, V.; Vrel, D.; Dubois, S. Crystal growth of TiC grains during SHS reactions. *J. Cryst. Growth* **2007**, 304, 481-486.
5. Zhang, L.; Hu, J.; Voevodin, A.A.; Fong, H. Synthesis of continuous TiC nanofibers and/or nanoribbons through electrospinning followed by carbothermal reduction. *Nanoscale* **2010**, 2, 1670-1673.
6. Suryanarayana, C.; Ivanov, E. Mechanochemical synthesis of nanocrystalline metal powders. Woodhead Publishing Series in Metals and Surface Engineering, *Advances in Powder Metallurgy* **2013** 42-68.
7. Jia, H.; Zhang, Z.; Qi, Z.; Liu, G.; Bian, X. Formation of nanocrystalline TiC from titanium and different carbon sources by mechanical alloying. *J. Alloys Compd.* **2009**, 472, 97-103.
8. Lohse, B.H.; Calka, A.; Wexler, D. Synthesis of TiC by controlled ball milling of titanium and carbon. *J. Mater. Sci.* **2006**, 42, 669-675.
9. Korchagin, M.A.; Gabdrashova, S.E.; Dudina, D.V.; Bokhonov, B.B.; Bulina, N.V.; Kuznetsov, V.L.; Ishchenko, A.V. Combustion characteristics and structure of carbon nanotube/titanium composites. *J. Therm. Anal. Calorim.* 2019, 137, 1903-1910.
10. Nouri, A.; Wen, C. Surfactants in Mechanical Alloying/Milling: A Catch-22 Situation. *Crit. Rev. Solid State Mater. Sci.* **2013**, 39, 81-108.
11. Alamolhoda, S.; Heshmati-Manesh, S.; Ataie, A.; Badiei, A. Role of process control agents on milling behavior of Al and TiO_2 powder mixture to synthesize TiAl/Al_2O_3 nano composite. *Int. J. Mod. Phys.: Conf.* **2012**, 5, 638-645.
12. Tokumitsu, K. Reduction of metal oxides by mechanical alloying method. *Solid State Ion.* **1997**, 101-103, 25-31.
13. Nouri, A.; Hodgson, P.D.; Wen, C.E. Study on the Role of Stearic Acid and Ethylene-bis-stearamide on the Mechanical Alloying of a Biomedical Titanium Based Alloy. *Metall. Mater. Trans. A* **2010**, 41, 1409-1420.
14. Schoenitz, M.; Zhu, X.; Dreizin, E.L. Carbide formation in Al–Ti mechanical alloys. *Scr. Mater.* **2005**, 53,1095-1099.
15. Jari Keskinen, A.P.; Rubin, J.; Ruuskanen, P. Carbide and hydride formation during mechanical alloying of titanium and aluminium with hexane. *Mater. Sci. Eng. A* **1995**, 196, 205-211.
16. Suzuki, T.S.; Nagumo, M. Metaestable intermediate phase formation at reaction milling of titanium and n-Heptane. *Scr. Metall. Mater.* **1995**, 32, 1215-1220.
17. Aguilar-Elguézabal, A.; Antúnez, W.; Alonso, G.; Delgado, F.P.; Espinosa, F.; Miki-Yoshida, M. Study of carbon nanotubes synthesis by spray pyrolysis and model of growth. *Diam. Relat. Mater.* **2006**, 15, 1329-1335.
18. Valenzuela-Muñiz, A.M.; Alonso-Nuñez, G.; Miki-Yoshida, M.; Botte, G.G.; Verde-Gómez, Y. High electroactivity performance in Pt/MWCNT and PtNi/MWCNT electrocatalysts. *Int. J. Hydrog. Energy* **2013**, 38, 12640-12647.

19. Rosado, G.; Verde, Y.; Valenzuela-Muñiz, A.M.; Barbosa, R.; Miki Yoshida, M.; Escobar, B. Catalytic activity of Pt-Ni nanoparticles supported on multi-walled carbon nanotubes for the oxygen reduction reaction. *Int. J. Hydrog. Energy* **2016**, 41, 23260-23271.
20. Gao, Y.Y.; Qiu, F.; Liu, T.S.; Chu, J.G.; Zhao, Q.L.; Jiang, Q.C. Effects of Carbon Source on TiC Particles' Distribution, Tensile, and Abrasive Wear Properties of In Situ TiC/Al-Cu Nanocomposites Prepared in the Al-Ti-C System. *Nanomaterials* **2018**, 8, 610.
21. Degen, T.; Sadki, M.; Bron, E.; König, U.; Nénert, G. The HighScore suite, *Difracción de polvo* **2014**, 29(S2), S13-S18.
22. Bolokang, A.S.; Motaung, D.E.; Arendse, C.J.; Muller, T.F.G. Formation of the metastable FCC phase by ball milling and annealing of titanium–stearic acid powder. *Adv. Powder Technol.* **2015**, 26, 632-639.
23. Saba, F.; Sajjadi, S.A.; Haddad-Sabzevar, M.; Zhang., F. Formation mechanism of nano titanium carbide on multi-walled carbon nanotube and influence of the nanocarbides on the load-bearing contribution of the nanotubes inner-walls in aluminum-matrix composites. *Carbon* **2017**, 115, 720-729.
24. Yan, M.; Qian, M.; Kong, C.; Dargusch, M.S. Impacts of trace carbon on the microstructure of as-sintered biomedical Ti-15Mo alloy and reassessment of the maximum carbon limit. *Acta Biomater.* **2014**, 10, 1014-1023.
25. Munir, K.S.; Li, Y.; Liang, D.; Qian, M.; Xu, W.; Wen, C. Effect of dispersion method on the deterioration, interfacial interactions and re-agglomeration of carbon nanotubes in titanium metal matrix composites. *Mater. Des.* **2015**, 88, 138-148.
26. Liu, Z.G.; Guo, J.T.; Ye, L.L.; Li, G.S.; Hu, Z.Q. Formation mechanism of TiC by mechanical alloying. *Appl. Phys. Lett.* 1994, 65, 2666-2668.
27. Yuan, Q.; Zheng, Y.; Yu, H. Synthesis of nanocrystalline Ti(C,N) powders by mechanical alloying and influence of alloying elements on the reaction. *Int. J. Refract. Met. Hard Mater.* **2009**, 27, 121-125.
28. Rahaei, M.B.; Yazdani rad, R.; Kazemzadeh, A.; Ebadzadeh, T. Mechanochemical synthesis of nano TiC powder by mechanical milling of titanium and graphite powders. *Powder Technol.* **2012**, 217, 369-376.
29. Adegbenjo, A.O.; Olubambi, P.A.; Potgieter, J.H.; Nsiah-Baafi, E.; Shongwe, M.B. Interfacial Reaction During High Energy Ball Milling Dispersion of Carbon Nanotubes into Ti_6Al_4V. *J. Mater. Eng. Perform.* **2017**, 26, 6047-6056.
30. Munir, K.S.; Li, Y.; Qian, M.; Wen, C. Identifying and understanding the effect of milling energy on the synthesis of carbon nanotubes reinforced titanium metal matrix composites. *Carbon* **2016**, 99 384-397.
31. Dorofeev, G.A.; Lubnin, A.N.; Lad'yanov, V.I.; Mukhgalin, V.V.; Puskkarev, B.E. Structural and phase transformations during ball milling of titanium in medium of liquid hydrocarbons. *Phys. Met. Metallogr.* **2014**, 115, 157-168.
32. Seelam, U.M.R.; Barkhordarian, G.; Suryanarayana, C. Is there a hexagonal-close-packed (hcp) → face-centered-cubic (fcc) allotropic transformation in mechanically milled Group IVB elements? *J. Mater. Res.* **2011**, 24, 3454-3461.
33. Momma, K.; Izumi, F. VESTA: a three-dimensional visualization system for electronic and structural analysis. *J. Appl. Crystallogr.* **2008**, 41, 653-658.
34. Mitchell, D.R.; Shaffer, B. Scripting-customized microscopy tools for Digital Micrograph. *Ultramicroscopy* **2005**, 103, 319-332.
35. Lehman, J.H.; Terrones, M.; Mansfield, E.; Hurst, K.E.; Meunier, V. Evaluating the characteristics of multiwall carbon nanotubes. *Carbon* **2011**, 49, 2581-2602.
36. Delhaes, P.; Couzi, M.; Trinquecoste, M.; Dentzer, J.; Hamidou, H.; Vix-Guterl, C. A comparison between Raman spectroscopy and surface characterizations of multiwall carbon nanotubes. *Carbon* **2006**, 44, 3005-3013.
37. Klein, M.V.; Holy, J.A.; Williams, W.S. Raman scattering induced by carbon vacancies inTiCx. *Phys. Rev. B* **1978**, 17, 1546-1556.
38. Amer, M.; Barsoum, M.W.; El-Raghy, T.; Weiss, I.; Leclair, S.; Liptak, D. The Raman spectrum of Ti_3SiC_2. *J. Appl. Phys.* **1998**, 84, 5817-5819.
39. Magnus, C.; Sharp, J.; Rainforth, W.M. The Lubricating Properties of Spark Plasma Sintered (SPS) Ti_3SiC_2 MAX Phase Compound and Composite. *Tribol.Trans.* **2019**, 63, 38-51.